NON-GAUSSIAN FLUCTUATION DYNAMICS*

Xin An

Department of Physics and Astronomy, University of North Carolina
Chapel Hill, NC 27599, USA

Received 31 July 2022, accepted 2 October 2022,
published online 14 December 2022

Recent progress of a general deterministic approach to the non-Gaussian fluctuation dynamics is reviewed, with an emphasis on the derivation of the fluctuation evolution equations and their phenomenological implication in heavy-ion collision experiments.

DOI:10.5506/APhysPolBSupp.16.1-A47

1. Introduction

Fluctuations are ubiquitous phenomena emerging on all length scales, from the cosmological length all the way to the size of the quark–gluon plasma created in heavy-ion collisions, where they could potentially play essential roles. In many situations, fluctuations are resulted from addition of independent and random sources on smaller scales and are approximately described by the Gaussian distribution, per the central limit theorem. In addition, the time scale of system evolution is usually much larger than the time scale of the fluctuation equilibration process, so fluctuations can also be well approximated as in equilibrium. Nonetheless, there are certain situations where fluctuations can significantly deviate from their Gaussian and/or equilibrium distribution, and these deviations arouse more and more interest in various physical subjects in recent years. A typical example, which will be focused on this work, is the event-by-event fluctuations of particle multiplicities in heavy-ion collision experiments. The shape of the multiplicity distribution for the observed particles (*e.g.*, net protons), characterized by its cumulants, carries important information about the collision process. For example, it was argued that in equilibrium, the higher-order cumulants are more sensitive to the critical point [1, 2], which may give rise to the non-monotonic energy dependence of the particle fluctuations in heavy-ion collisions — an intriguing hint of the QCD critical point [3]. However, since the fireballs created by the collisions of two ultrarelativistic nuclei are short-lived and rapidly expanding, it would be natural to expect that the

* Presented at the 29th International Conference on Ultrarelativistic Nucleus–Nucleus Collisions: Quark Matter 2022, Kraków, Poland, 4–10 April, 2022.

fluctuations may fall out of equilibrium. Thus, the argument in Refs. [1, 2] based on the equilibrium theory needs to be amended to incorporate the non-equilibrium effects of non-Gaussian fluctuations — the major motivation of Refs. [4, 5]. In this contribution, the progress achieved in Ref. [4] will be reviewed in Sec. 2. Additional numerical results will be presented and discussed in Sec. 3. These works altogether constitute an integral part of the BEST framework [6] for interpreting the forthcoming experimental results from the second phase of the RHIC Beam Energy Scan program.

2. Fluctuation evolution equations

The *Langevin equations* for a set of stochastic fields ψ_is, with the index $i = (i_1, i_2, \ldots)$ labeling both the variables and their associated space coordinates (if applicable), read

$$\partial_t \psi_i = F_i + \xi_i \,, \tag{1}$$

where F_i and ξ_i are the drift force and random force (noise), respectively. The noise is assumed to be Gaussian, *i.e.*,

$$\langle \xi_{i_1}(t_1)\xi_{i_2}(t_2)\rangle = 2Q_{i_1 i_2}\delta(t_1 - t_2) \,, \tag{2}$$

and its amplitude Q_{ij}, known as the Onsager matrix, is set by the fluctuation–dissipation relation. One can convert the Langevin equations (1) into the *Fokker–Planck equation* for the probability distribution function of the stochastic fields, $P(\psi_i; t)$ [7],

$$\partial_t P = \Big(-F_i P + (Q_{ij}P)_{,j}\Big)_{,i} \,, \tag{3}$$

where $(\ldots)_{,i} = \delta(\ldots)/\delta\psi_i$ [1]. The Fokker–Planck equation solves two problems the Langevin equation suffered from the problem of *infinite noise* due to the divergence of δ-function in Eq. (2) when $t_1 \to t_2$; and the problem of *multiplicative noise* due to the ambiguity of the noise amplitude Q_{ij} in the continuous limit $\Delta t \to 0$, where Δt is the discretized time increment of the evolution. The divergence in the first problem can be regularized analytically using the renormalization techniques [8–10], while the ambiguity in the second problem can be eliminated by specifying the discretization prescription, *e.g.*, Ito's prescription as in Eq. (3).

The cumulant generating functional, $\mathcal{W}[\mu_i]$, is defined through

$$\mathrm{e}^{\mathcal{W}[\mu_i]} = \Big\langle \mathrm{e}^{\mu_i\psi_i} \Big\rangle \equiv \int \mathcal{D}\psi P \, \mathrm{e}^{\mu_i\psi_i} \,, \tag{4}$$

which can be expanded in a series of the external sources μ_is

[1] This equation is invariant under $Q_{ij} \to Q_{ij} + \Omega_{ij}$, where $\Omega_{ij} = -\Omega_{ji}$ is the antisymmetric matrix obtained from the Poisson bracket of stochastic fields [7].

$$\mathcal{W} = \sum_{n=1}^{\infty} \frac{1}{n!} G^{\mathrm{c}}_{i_1 \dots i_n} \mu_{i_1} \dots \mu_{i_n} \,, \tag{5}$$

where the expansion coefficient $G^{\mathrm{c}}_{i_1 \dots i_n} \equiv G^{\mathrm{c}}_n \equiv \delta \mathcal{W} / \delta \mu_{i_1} \dots \delta \mu_{i_n} |_{\mu=0}$ is the n^{th} cumulant. Using Eqs. (3) and (4), one arrives at the evolution equation for $\mathcal{W}[\mu_i]$

$$\partial_t \mathcal{W} = \mathrm{e}^{-\mathcal{W}} \left(\mu_i F_i + \mu_i \mu_j Q_{ij} \right) \mathrm{e}^{\mathcal{W}} \,, \tag{6}$$

where $F_i = F_i(\delta/\delta\mu_i)$, $Q_{ij} = Q_{ij}(\delta/\delta\mu_i)$. Substituting Eq. (5) into (6), one can readily obtain the evolution equation for cumulant G^{c}_n. However, these equations are not in closed form, *i.e.*, the equations for lower-order cumulants also depend on higher-order cumulants. Fortunately, in certain regimes where some parameters are legitimately small, these equations can be systematically truncated. We introduced two such parameters. The parameter ε, which is inversely proportional to the uncorrelated degrees of freedom, controls the loop expansion. Another parameter δ, identified as the Knudsen number in hydrodynamics, controls the gradient expansion. Although each of them plays its own role, they are not independent and are indeed related by $\varepsilon \sim \delta^3$ in hydrodynamics. Assigning the following power counting:

$$F_i \sim \delta^2 \,, \qquad Q_{ij} \sim \delta^2 \varepsilon \,, \qquad G^{\mathrm{c}}_n \sim \varepsilon^{n-1} \,, \tag{7}$$

and keeping the leading terms ($\sim \delta^2 \varepsilon^{n-1}$) that turn out to be connected tree-level diagrams, we arrive at the truncated and iteratively solvable equations, schematically formulated in the form of

$$\partial_t G^{\mathrm{c}}_n = \mathscr{F}_{\mathrm{tree}}[\{G^{\mathrm{c}}_n, G^{\mathrm{c}}_{n-1}, \dots, G^{\mathrm{c}}_2, \langle \psi \rangle\}] \tag{8}$$

and diagrammatically represented in Fig. 1. Their explicit forms can be found in Refs. [4, 5].

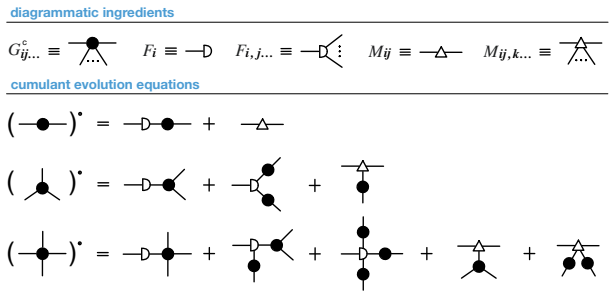


Fig. 1. Diagrammatic representation of Eq. (8) (or Eq. (10)) for $n = 2, 3, 4$ in terms of the diagrammatic ingredients introduced in this figure. The dot on the left-hand side denotes the time derivative ∂_t.

If the variables $\psi_{i_1}, \ldots, \psi_{i_n}$ are fields defined locally in continuous real space at $\boldsymbol{x}_1, \ldots, \boldsymbol{x}_n$, it may be more convenient to analyze Eq. (8) in the wave-vector space. To this end, we introduced a novel *multi-point* Wigner function [4]

$$W_n^{\mathrm{c}}(\boldsymbol{x}, \boldsymbol{q}_1, \ldots, \boldsymbol{q}_n) = \int \left[\prod_{i=1}^{n} \mathrm{d}^3\boldsymbol{y}_i \, \mathrm{e}^{-i\boldsymbol{q}_i\cdot\boldsymbol{y}_i}\right] \delta^{(3)}\left(\frac{1}{n}\sum_{i=1}^{n}\boldsymbol{y}_i\right) G_n^{\mathrm{c}}(\boldsymbol{x}_1, \ldots, \boldsymbol{x}_n)\,, \tag{9}$$

where $\boldsymbol{q}_i$ is the wave-vector conjugate to $\boldsymbol{y}_i \equiv \boldsymbol{x}_i - \boldsymbol{x}$ and $\boldsymbol{x} = \sum_{i=1}^{n}\boldsymbol{x}_i/n$. Under this Wigner transform, we imposed the constraint $\sum_{i=1}^{n}\boldsymbol{y}_i = 0$; as a consequence, $\boldsymbol{q}_i$s are not independent and must also sum to zero after an appropriate shift. Obviously, Eq. (9) reproduces the traditional definition of the Winger function when $n = 2$. Using Eq. (9), one can represent Eq. (8) in the wave-vector space. We defer its presentation in a specific problem discussed in Sec. 3. For the *confluent* formulation of non-Gaussian fluctuations in relativistic fluid, see Ref. [5].

3. Non-Gaussian fluctuation dynamics of diffusive charge

In this section, we apply our general formalism to a specific problem — the evolution of diffusive charge, using the translation given by Table 1. In this problem, the stochastic variable, charge density $n(\boldsymbol{x})$, is defined in continuous space, the Onsager matrix Q_{ij} is related to conductivity λ through the fluctuation–dissipation relation, and the drift force F_i is given by the divergence of a diffusion current whose constitutive relation, $\lambda\boldsymbol{\nabla}\alpha$, where α is the chemical potential per temperature, can be determined by the second law of thermodynamics.

Table 1. Translation of general formalism to the problem of diffusive charge.

Quantities	General	Diffusive charge
Variable	ψ_i	$n(\boldsymbol{x})$
Variable index	$i, j, k,$ *etc.*	$\boldsymbol{x}, \boldsymbol{y}, \boldsymbol{z},$ *etc.*
Onsager matrix	Q_{ij}	$\boldsymbol{\nabla}_{\boldsymbol{x}}\lambda\boldsymbol{\nabla}_{\boldsymbol{y}}\,\delta^{(3)}_{\boldsymbol{x}\boldsymbol{y}}$
Drift force	F_i	$\boldsymbol{\nabla}_{\boldsymbol{x}}\lambda\boldsymbol{\nabla}_{\boldsymbol{x}}\alpha$

Applying the translation in Table 1 to Eq. (8) and using Eq. (9), one immediately obtains the evolution equations for the diffusive charge cumulants in the wave-vector space. The first few equations for $n = 2, 3, 4$ read (*cf.* Fig. 1)

$$\begin{aligned}
\partial_t W_2(\boldsymbol{q}_1) &= -2\left[\gamma\boldsymbol{q}_1^2 W_2(\boldsymbol{q}_1) + \lambda\boldsymbol{q}_1\cdot\boldsymbol{q}_2\right]_{\overline{12}}\,,\\
\partial_t W_3(\boldsymbol{q}_1, \boldsymbol{q}_2) &= -3\left[\gamma\boldsymbol{q}_1^2 W_3(\boldsymbol{q}_1, \boldsymbol{q}_2) + \gamma'\boldsymbol{q}_1^2 W_2(\boldsymbol{q}_2)W_2(\boldsymbol{q}_3)\right.\\
&\quad \left. +2\lambda'\boldsymbol{q}_1\cdot\boldsymbol{q}_2 W_2(\boldsymbol{q}_3)\right]_{\overline{123}}\,,
\end{aligned}$$

$$\begin{aligned}\partial_t W_4^{\rm c}(\boldsymbol{q}_1,\boldsymbol{q}_2,\boldsymbol{q}_3) \;=\; & -4\big[\gamma \boldsymbol{q}_1^2 W_4^{\rm c}(\boldsymbol{q}_1,\boldsymbol{q}_2,\boldsymbol{q}_3) + 3\gamma' \boldsymbol{q}_1^2 W_2(\boldsymbol{q}_2) W_3(q_3,\boldsymbol{q}_4) \\ & + \gamma'' \boldsymbol{q}_1^2 W_2(\boldsymbol{q}_2) W_2(\boldsymbol{q}_3) W_2(\boldsymbol{q}_4) + 3\lambda' \boldsymbol{q}_1\cdot\boldsymbol{q}_2 W_3(\boldsymbol{q}_3,\boldsymbol{q}_4) \\ & + 3\lambda'' \boldsymbol{q}_1\cdot\boldsymbol{q}_2 W_2(\boldsymbol{q}_3) W_2(\boldsymbol{q}_4)\big]_{\overline{1234}}\,, \end{aligned} \tag{10}$$

where $\gamma = \lambda\alpha'$, $\alpha' \equiv \partial\alpha/\partial n$ and $\overline{1\ldots n}$ denotes the sum over all $n!$ permutations of $\boldsymbol{q}_1,\ldots,\boldsymbol{q}_n$ divided by $n!$. Equations (10) are solved by $W_2^{\rm eq} = 1/\alpha'$, $W_3^{\rm eq} = -\alpha''/\alpha'^3$, $W_4^{\rm c,eq} = (3\alpha''^2 - \alpha'\alpha''')/\alpha'^5$ in equilibrium, as expected from thermodynamic calculations.

In the critical regime where the correlation length ξ is still much less than the fluctuation scale $q^{-1} \equiv |\boldsymbol{q}|^{-1}$ but becomes much larger than all other microscopical lengths such as the inverse of temperature, *i.e.*, $T^{-1} \ll \xi \ll q^{-1}$, all thermodynamic and transport quantities will acquire their dependence on the correlation length (which serves as a UV cutoff of fluctuations). For the dynamical universality class of Model H in three dimensions, we have approximately [5]

$$\alpha^{(n)} \sim \xi^{\frac{n-5}{2}}\,,\quad \lambda^{(n)} \sim \xi^{\frac{n+2}{2}}\,,\quad \gamma^{(n)} \sim \xi^{\frac{n-2}{2}}\,,\quad W_n^{\rm c} \sim \xi^{\frac{5n-6}{2}}\,,\quad \partial_t W_n^{\rm c} \sim q^2 \xi^{\frac{5n-8}{2}}\,. \tag{11}$$

The last relation in Eq. (11) says that all terms presented in each equation of (10) are in the same power of correlation length, demonstrating their equal importance near the critical point.

To see how Eqs. (10) work in practice, let us consider the problem of baryon charge cumulant evolution in the crossover region near the QCD critical point (see Fig. 2). Our purpose would be illustrating the robust phenomenological consequence of Eqs. (10). To this end, we postulate the following assumptions which simplify our simulations without losing the main features of the results. First, when establishing the dependence of the correlation length ξ on baryon chemical potential μ and temperature T, we use a mapping $\xi(\mu,T) = \xi_{\rm Ising}(r(\mu,T), h(\mu,T))$ from the Ising model, where r is the Ising temperature and h is the Ising magnetic field, and assume the mapping is linear and orthogonal around the critical point $(\mu_{\rm c}, T_{\rm c})$, *i.e.*, $\mu - \mu_{\rm c} \sim r$ and $T - T_{\rm c} \sim h$. Second, the evolution trajectories, rather complicated in reality, are assumed to be perpendicular to the crossover line (see the right panel of Fig. 2). Third, the system is assumed to be in equilibrium at the initial time $t_{\rm i}$, *i.e.*, the moment when the system just enters the critical region and assumed to freeze out before the final time $t_{\rm f}$, *i.e.*, the moment when the system leaves the critical region. Fourth, the system is assumed to be isotropic such that $W_n^{\rm c}$'s depend only on $n(n-1)/2$-independent scalar invariants, $\boldsymbol{q}_i\cdot\boldsymbol{q}_j$, $i<j$, which are all set to q^2 for simplicity [4].

Simulating Eqs. (10) using the above assumptions, we find the contour maps of cumulants $W_{n=2,3,4}^{\rm c}$ in the critical region, shown in Fig. 3. The top panel shows the contours of cumulants in equilibrium, which are symmetric

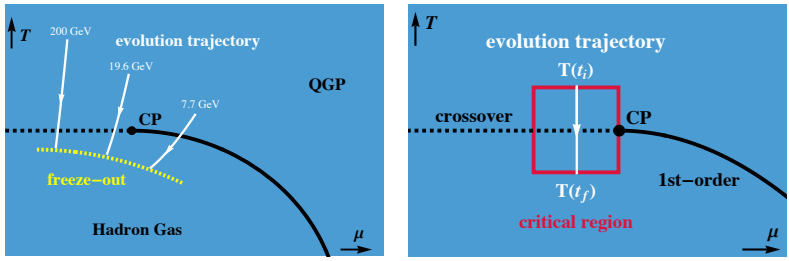


Fig. 2. (Color online) QCD phase diagram (left) and the zoomed-in critical region near the QCD critical point (right). The black dashed and solid curve is the crossover and first-order phase transition line. The white lines represent the evolution trajectories of each collision event mapped to the QCD phase diagram, with arrows indicating the time evolution direction. The yellow/pale gray dashed curve is the freeze-out line where observables are measured. The critical region studied in Figs. 3 and 4 is bounded by the red/gray square.

to the crossover line due to the aforementioned simplifications. The bottom panel shows a particular example (*i.e.*, $q = 0.1$) [2], where the cumulants are out of equilibrium. In this case, the contours are significantly distorted

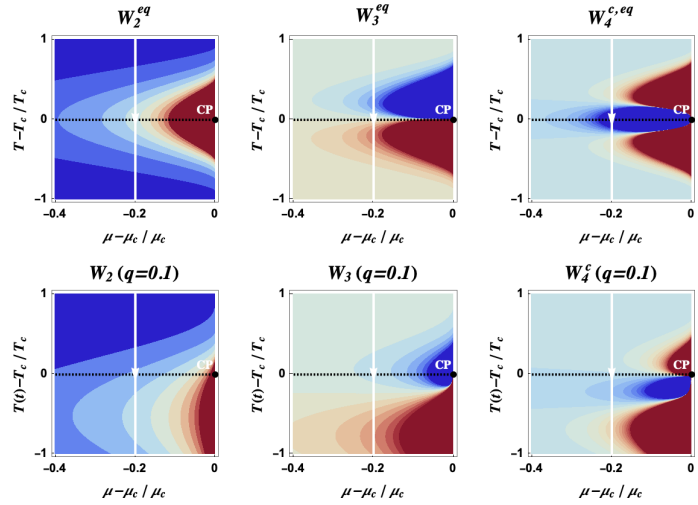


Fig. 3. Contour maps of cumulants $W^{\rm c}_{n=2,3,4}$ in equilibrium (top panel, $q \to \infty$) and out of equilibrium (bottom panel, $q = 0.1$).

as if they are dragged toward the time evolution direction. In other words, although the dynamic cumulants keep approaching their instantaneous equilibrium values, they still retain memories of their past evolution history[3].

[2] Here, we used arbitrary units, which are not specified thereby.

[3] A similar study can be found in Ref. [11] for the homogeneous mode that is independent of the scale q.

Focusing on the fourth cumulant W_4^c, we plot the contours for different q's in Fig. 4. We find that cumulants are closer to equilibrium on a smaller scale (*e.g.*, $q = 0.3$), while retaining a longer memory of the past on a larger scale (*e.g.*, $q = 0.1$). This is a consequence of causality: on a larger spatial scale, fluctuations need a longer time to equilibrate. When $q \to 0$ (infinitely large scale), fluctuations will be completely suppressed due to the conservation of charges and remain as if they were at the initial time (which, of course, are also suppressed).

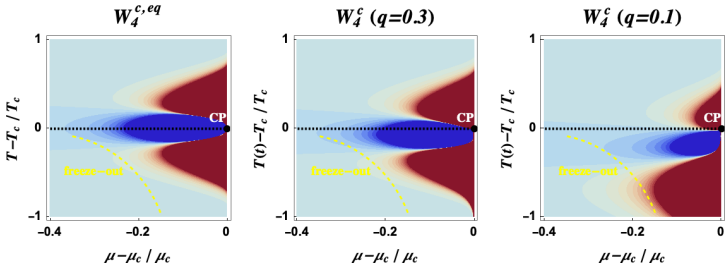


Fig. 4. (Color online) Contour maps of fourth cumulant W_4^c at $q \to \infty$ (left), $q = 0.3$ (middle) and $q = 0.1$ (right) in the critical region. The freeze-out line (yellow dashed curve) is arbitrarily chosen for illustration purpose.

The fourth cumulant W_4^c is of particular interest to us, since its equilibrium value possesses more sensitivity to the critical point comparing to the lower-order cumulants. If one reads off its value along the freeze-out line (yellow dashed curve) in Fig. 4, one finds its expected non-monotonicity as a function of baryon chemical potential in Fig. 5. Noting that the baryon chemical potential is inversely related to the collision energy, Fig. 5 is qualitatively consistent with the experiment data reported in Ref. [3]. More interestingly, one finds that the curve for smaller q (red/black) might be shifted toward large baryon chemical potential more significantly compared to the one for larger q (blue/gray). That is to say, the non-equilibrium effect,

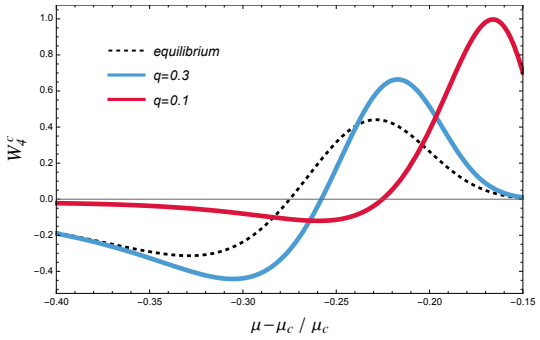


Fig. 5. The dependence of W_4^c on baryon chemical potential μ along the freeze-out line in Fig. 4, at $q \to \infty$ (equilibrium), $q = 0.3$ and $q = 0.1$ respectively.

largely coming from the fluctuations with wave vectors around $q \sim 0.1$–0.3, might shift the curve predicted by the equilibrium theory toward the lower collision energy. As a reminder, one should not compare the values here quantitatively, as our results are only for illustration purpose.

4. Summary

In this contribution, we reviewed a general deterministic approach to non-Gaussian fluctuation dynamics. This novel approach is established with controllable perturbative loop/gradient expansion and the multi-point Wigner function. In this approach, we derived the general evolution equations for cumulants and demonstrated their robust phenomenological implication via the problem of diffusive charge near the QCD critical point. Our numerical results suggest that the non-equilibrium effect to cumulants needs to be taken into account for a rigorous quantitative comparison with the experimental results. As for the future, the cumulant evolution equations need to be implemented in a more realistic setup, and our formalism is yet to incorporate all non-Gaussian hydrodynamic fluctuations with their freeze-out prescriptions [5, 8, 9, 12].

This work is supported by the U.S. Department of Energy, Office of Science, Office of Nuclear Physics, within the framework of the Beam Energy Scan Theory (BEST) Topical Collab. and grant No. DE-FG0201ER41195.

REFERENCES

[1] M. Stephanov, *Phys. Rev. Lett.* **102**, 032301 (2009).
[2] M. Stephanov, *Phys. Rev. Lett.* **107**, 052301 (2011).
[3] STAR Collaboration (J. Adam *et al.*), *Phys. Rev. Lett.* **126**, 092301 (2021).
[4] X. An, G. Başar, M. Stephanov, H.-U. Yee, *Phys. Rev. Lett.* **127**, 072301 (2021).
[5] X. An, G. Başar, M. Stephanov, H.-U. Yee, to appear.
[6] X. An *et al.*, *Nucl. Phys. A* **1017**, 122343 (2022).
[7] J. Zinn-Justin, *Int. Ser. Monogr. Phys.* **113**, 1 (2002).
[8] X. An, G. Başar, M. Stephanov, H.-U. Yee, *Phys. Rev. C* **100**, 024910 (2019).
[9] X. An, G. Başar, M. Stephanov, H.-U. Yee, *Phys. Rev. C* **102**, 034901 (2020).
[10] X. An, *Nucl. Phys. A* **1005**, 121957 (2021).
[11] S. Mukherjee, R. Venugopalan, Y. Yin, *Phys. Rev. C* **92**, 034912 (2015).
[12] M. Pradeep, K. Rajagopal, M. Stephanov, Y. Yin, *Phys. Rev. D* **106**, 036017 (2022), arXiv:2204.00639 [hep-ph].